Hindawi
Mathematical Problems in Engineering
Volume 2020, Article ID 1485937, 14 pages
https://doi.org/10.1155/2020/1485937

Research Article

An Improved VMD-Based Denoising Method for Time Domain Load Signal Combining Wavelet with Singular Spectrum Analysis

Jingjing Fu, Fuyou Cai, Yonghao Guo, Hongda Liu, and Wentie Niu

School of Mechanical Engineering, Tianjin University, Tianjin 300350, China

Correspondence should be addressed to Wentie Niu; niuwentie@tju.edu.cn

Received 11 December 2019; Revised 9 April 2020; Accepted 15 April 2020; Published 29 April 2020

Academic Editor: Sylwester Samborski

Measured load data play a crucial role in the fatigue durability analysis of mechanical structures. However, in the process of signal acquisition, time domain load signals are easily contaminated by noise. In this paper, a signal denoising method based on variational mode decomposition (VMD), wavelet threshold denoising (WTD), and singular spectrum analysis (SSA) is proposed. Firstly, a simple criterion based on mutual information entropy (MIE) is designed to select the proper mode number for VMD. Detrended fluctuation analysis (DFA) is adopted to obtain the noise level of the noisy signal, which can optimize the selection of MIE threshold. Meanwhile, the noisy signal is adaptively decomposed into band-limited intrinsic mode functions (BLIMFs) by using VMD. In addition, weighted-permutation entropy (WPE) is applied to divide the BLIMFs into signal-dominant BLIMFs and noise-dominant BLIMFs. Then, the signal-dominant BLIMFs are reconstructed with the noise-dominant BLIMFs processed by WTD. Finally, SSA is implemented for the reconstructed signal. Experimental results of synthetic signals demonstrate that the presented method outperforms the conventional digital signal denoising methods and the related methods proposed recently. Effectiveness of the proposed method is verified through experiments of the measured load signals.

1. Introduction

Fatigue failure is one of the main causes of mechanical failure. Thus, it is of great significance to analyze the fatigue durability of the mechanical structure [1]. The basis of durability design of agricultural vehicles is to obtain time domain load signals, which can reflect the real working condition. Usually, measured signals are nonstationary and contain a lot of noise due to the complex and changeable working environment, which makes it meaningless to apply measured signals directly to durability analysis. Therefore, it is of great significance to effectively remove the noise in time domain load signals for the durability analysis of agricultural machinery.

There are many general signal denoising methods, whose basic idea is to extract and reconstruct useful signal components through some criteria [2, 3]. Common signal decomposition methods include wavelet transform (WT), empirical mode decomposition (EMD), and variational mode decomposition (VMD). WT can decompose the signal into different frequencies through multiscale analysis and have good time-frequency localization characteristics. Donoho and Johnstone [4] proposed a threshold denoising method based on WT and achieved good results. Therefore, it has been applied in many fields, such as machinery [5], biomedicine [6], and chemistry [7]. However, wavelet threshold denoising (WTD) has poor denoising performance on the signal with low signal-to-noise ratio. Because the measured signal usually contains a lot of background noise, the performance of WTD is not ideal [8]. EMD was put forward by Huang et al. [9] in 1998. Compared with WT, it can adaptively decompose the signal into a series of intrinsic mode functions (IMFs) without much prior information. Therefore, it has been widely used in signal denoising [10–12] and analysis [13, 14]. However, the defects of EMD, such as mode aliasing [15] and end effect [16], restrict its wide application. For this reason, scholars have proposed improved methods of EMD, such as EEMD [17] and CEEMD [18]. However, similar to EMD, the improved methods based on EMD are all iterative algorithms, which

will inevitably produce the error accumulation phenomenon [19], and lack solid mathematical foundation [20].

In 2014, Dragomiretskiy and Zosso [21] proposed the variational mode decomposition (VMD), which is a non-iterative and adaptive signal processing method. Compared with the method based on EMD, it has a solid mathematical theoretical foundation, and it can avoid the error accumulation phenomenon. VMD-based denoising methods have been used in many fields, such as underwater acoustic signal [22], ship-radiated noise [23], seismic signal [24], and laser radar [25]. It is worth noting that the key problem of signal denoising with VMD is the determination of the mode number K and relevant modes. If we use trial and error to get the optimal mode number K, it will need dozens of operations and waste a lot of time. Therefore, the parameter values are usually determined based on experience and convenience, which seriously affects the denoising performance of VMD. For this reason, researchers have proposed many algorithms to select the mode number. For example, Liu et al. [26] determined the mode number by detrend fluctuation analysis (DFA) through a large number of simulation experiments and finally achieved a good denoising performance. Lei et al. [27] proposed a hybrid algorithm combining VMD and WTD and selected the mode number for VMD through the decomposition results of EMD. In addition, the proposed denoising algorithm is shown to be able to effectively recognize different cast speeds. Li et al. [28] proposed an improved VMD (IVMD), where the mode number is determined by a frequency-aided method. IVMD as a novel algorithm combining SE was first proposed for feature extraction of S-RN signals. At present, the main methods of selecting relevant modes are correlation coefficient [22], permutation entropy [29], approximate entropy [30], Hausdorff distance [31], Euclidean distance [32], etc. However, pure VMD denoising can not only remove the high-frequency noise but also reduce the effective high-frequency information. Some scholars have proposed to use the wavelet threshold method to remove noise components from high-frequency components and reconstruct the signal [27]. However, WTD cannot completely remove the high-frequency noise, and with the change of operation conditions, the low-frequency signal will be adulterated with low-frequency interharmonics [33], so the performance of the abovementioned denoising method is not ideal. Singular spectrum analysis (SSA) proposed by Broomhead and King [34] can decompose signals into a series of independent and meaningful principal components [35]. Therefore, SSA may be an effective method to identify useful signals from noise [36].

In this paper, DFA is used to get the noise level of the noisy signal, and mutual information entropy (MIE) is used to determine the mode number for adaptive VMD denoising. Meanwhile, the advantages of WTD and SSA are effectively absorbed. Firstly, the noise level of the noisy signal is obtained by using DFA [37], and the mode number for VMD is obtained by using MIE. At the same time, the noisy signal is decomposed into a series of BLIMFs by VMD. Next, weighted-permutation entropy (WPE) is adopted to distinguish between signal-dominated BLIMFs and noise-dominated BLIMFs. Then, the signal-dominant BLIMFs are reconstructed with the noise-dominant BLIMFs, which have been denoised by WTD. Finally, SSA is implemented for the reconstructed signal. Simulation and experimental results show the effectiveness and superiority of the proposed method.

The rest of this paper is organized as follows. The related theories, including VMD, WPE, WTD, and SSA, are introduced in Section 2. The proposed denoising method is presented in Section 3. In Section 4, the proposed method is compared with other existing methods, and the superiority of the proposed method is proved. In Section 5, the proposed method is applied to measured load signals. Finally, conclusions are drawn in Section 6.

2. Methodology

2.1. Brief Description of the VMD Algorithm [21]. The VMD algorithm can decompose any signal into a series of BLIMFs by iteratively searching the optimal solution of the variational model. Each mode is compact around its respective center frequency ω_k. In this algorithm, the intrinsic mode function (IMF) is redefined as an amplitude-modulated-frequency-modulated (AM-FM) signal, which can be written as

$$u_k(t) = A_k(t)\cos\left(\phi_k(t)\right), \tag{1}$$

where phase $\phi_k(t) > 0$ is a nondecreasing function and $A_k(t)$ is the instantaneous amplitude of $u_k(t)$.

Both the instantaneous amplitude $A_k(t)$ and the instantaneous frequency $\omega_k(t) = \phi_k'(t)$ vary slower than the phase $\phi_k(t)$ so that pseudostationarity can be assumed. In order to search for suitable $u_k(t)$ and $\omega_k(t)$, VMD algorithm is required to solve the following constrained variational problem:

$$\begin{aligned} &\min_{\{u_k\},\{\omega_k\}} \quad \left\{\sum_{k=1}^{K}\left\|\partial_t\left[\left(\delta(t)+\frac{j}{\pi t}\right)*u_k(t)\right]e^{-j\omega_k t}\right\|_2^2\right\} \\ &\text{s.t.} \qquad \sum_{k=1}^{K} u_k = f, \end{aligned} \tag{2}$$

where $\{u_k\}$ and $\{\omega_k\}$ are modes and their center frequency, respectively, K is the mode number, ∂_t represents the gradient with respect to t, $\delta(t)$ denotes the unit impulse function, $*$ is the convolution symbol, and f is the original signal to be decomposed.

In order to render the problem unconstrained, a quadratic penalty α and a Lagrangian multiplier λ are taken into consideration. The augmented Lagrangian is expressed as follows:

$$\begin{aligned} L\left(\{u_k\},\{\omega_k\},\lambda\right) = \alpha\sum_{K}\left\|\partial_t\left[\left(\delta(t)+\frac{j}{\pi t}\right)*u_k(t)\right]e^{-j\omega_k t}\right\|_2^2 + \\ \left\|f(t)-\sum_{K}u_k(t)\right\|_2^2 + \langle\lambda(t), f(t)-\sum_{K}u_k(t)\rangle. \end{aligned} \tag{3}$$

When the alternate direction method of multipliers (ADMM) is used to solve the problem, u_k^{n+1}, ω_k^{n+1}, and λ^{n+1} are updated until the optimal solution of the variational constrained problem is obtained. The modal component $\hat{u}_k^{n+1}$ in the frequency domain can be expressed as

$$\hat{u}_k^{n+1}(\omega) = \frac{\hat{f}(\omega) - \sum_{i\neq k}\hat{u}_i(\omega) + (\hat{\lambda}(\omega)/2)}{1 + 2\alpha(\omega - \omega_k)^2}, \tag{4}$$

where $\hat{u}$ is the Fourier transform of u. Equation (4) is the Fourier representation of a Wiener filter with power spectrum prior $1/(\omega - \omega_k)^2$. It ensures that the VMD algorithm has a good noise robustness.

Similarly, the center frequency ω_k^{n+1} can be expressed as

$$\omega_k^{n+1}(\omega) = \frac{\int_0^\infty \omega\left|\hat{u}_k(\omega)\right|^2 \mathrm{d}\omega}{\int_0^\infty \left|\hat{u}_k(\omega)\right|^2 \mathrm{d}\omega}. \tag{5}$$

The stopping condition of the iteration is

$$\sum_{k=1}^{K} \frac{\left\|\hat{u}_k^{n+1} - \hat{u}_k^n\right\|_2^2}{\left\|\hat{u}_k^n\right\|_2^2} < e, \tag{6}$$

where e is a given value.

2.2. A Parameter-Adaptive VMD Method. Compared with EMD and its improved algorithm, VMD has solid theoretical derivation and stronger robustness for data sampling and noise. However, two crucial parameters in the decomposition algorithm need to be resolved, i.e., the decomposition mode number K and the quadratic penalty α. A relatively moderate value of α is recommended to be 2000 [21].

In order to avoid the impact of overbinning or underbinning on the VMD denoising, the appropriate number K must be selected. MIE [38] can be used to represent the statistical dependence of two random variables, so as to reflect the degree of correlation. The expression is addressed as follows:

$$\mathrm{MIE}(X,Y) = \sum_{i=1}^{r}\sum_{j=1}^{s} p(x_i, y_j)\,\mathrm{lb}\frac{p(x_i, y_j)}{p(x_i)p(y_j)}, \tag{7}$$

where X and Y represent different random variables, $p(x_i, y_j)$ is the joint probability distribution, $p(x_i)$ and $p(y_i)$ are the marginal probability distributions, r and s are the length of X and Y, respectively, and lb denotes the binary logarithm.

The stronger the correlation between X and Y, the greater MIE will be obtained. In this paper, The MIEs between BLIMF_l ($l = 1, 2, \ldots, K$) and the noisy signal are designed to select the number K. The MIE can be normalized as

$$\delta_l = \frac{\mathrm{MIE}_l}{\max(\mathrm{MIE}_l)}, \tag{8}$$

where MIE_l is the MIE between BLIMF_l ($l = 1, 2, \ldots, K$) and the noisy signal.

When the minimum of δ_l ($l = 1, 2, \ldots, K$) is less than or equal to a specified threshold value δ, it can be considered that the decomposed mode does not contain important information, and the number K will be taken as the optimal mode number of VMD. However, the more noise in the noisy signal, the greater the MIE between the noise-dominant BLIMFs and the noisy signal. Therefore, a single threshold cannot meet all signals with different noise levels. In order to widen the application scope of this method, DFA is introduced to optimize the selection of threshold through a large number of simulation experiments.

The scaling exponent α_0 [39] provides a quantitative measure of the temporal correlations that exists in the time series. It can also be viewed as an indicator that describes the "roughness" of the original time series: the larger the value of α_0, the smoother the time series [39]. In this paper, through a large number of simulation experiments, the scaling exponent α_0 is used to represent the noise level of the noisy signal. The appropriate threshold value is selected to determine the mode number of VMD, and the selection expression of the threshold value proposed in this paper is described as follows:

$$\delta = \begin{cases} 0.3, & \alpha_0 < 0.6, \\ 0.05, & 0.6 \le \alpha_0 < 0.8, \\ 0.02, & 0.8 \le \alpha_0 < 1.2, \\ 0.015, & 1.2 \le \alpha_0 < 1.5, \\ 0.01, & 1.5 \le \alpha_0 < 1.8, \\ 0.005, & 1.8 \le \alpha_0. \end{cases} \tag{9}$$

2.3. Division of BLIMFs Based on WPE [40]. Permutation entropy (PE), proposed by Bandt and Pompe [41], can represent the complexity of time series. It is a nonlinear dynamic method to analyze the complexity of the system. Its algorithm is fast and easy to implement. However, PE simply arranges the components in the phase space vector, which results in the loss of amplitude information in the time series. The weighted-permutation entropy (WPE) proposed by Fadlallah et al. [40] can consider the amplitude information of time series on the basis of PE, which significantly improves the robustness and antinoise performance of PE. WPE can be described as follows:

(1) For a given time series $\{z_t\}_{t=1}^n$, the matrix of phase space reconstruction can be expressed as

$$\mathbf{Z} = \begin{bmatrix} z_1 & z_{1+\tau} & \cdots & z_{1+(m-1)\tau} \\ z_2 & z_{2+\tau} & \cdots & z_{2+(m-1)\tau} \\ \vdots & \vdots & \vdots & \vdots \\ z_c & z_{c+\tau} & \cdots & z_n \end{bmatrix}, \tag{10}$$

where τ is the time delay, m is the embedding dimension, and c is the number of phase space components, $c = n - (m-1)\tau$.

(2) The weight of each row of $\mathbf{Z}$ is calculated as

$$w_i = \frac{1}{m}\sum_{j=1}^{m}\left[z_{i+(j-1)\tau} - \overline{z}_i\right]^2, \quad i = 1, 2, \ldots, c, \tag{11}$$

where $\overline{z}_i$ is the mean value of each row, $\overline{z}_i = (1/m)\sum_{i=1}^{m} z_{i+(j-1)\tau}$.

(3) Each row of $\mathbf{Z}$ can be arranged in ascending order:

$$z_{i+(k_1-1)\tau} \le z_{i+(k_2-1)\tau} \le \cdots \le z_{i+(k_l-1)\tau} \le \cdots \le z_{i+(k_m-1)\tau}, \tag{12}$$

where k_l is the column index of each element in the ith row.

(4) After that, each row is arranged in ascending order, and a group of permutations can be obtained. Since the embedding dimension is m, there will be $m!$ possible permutations. We calculated the appearing number of every permutation n_a, $1 \le a \le m!$, and the weighted relative frequency of each permutation can be expressed as

$$p_w(a) = \frac{w_i n_a}{\sum_{i=1}^{c} w_i}. \tag{13}$$

(5) Then, the WPE can be designated as follows:

$$H_w(m) = -\sum_{i=1}^{m!} p_w(a)\ln p_w(a), \tag{14}$$

and the WPE of order can be normalized as

$$h_w = \frac{H_w(m)}{\ln(m!)}. \tag{15}$$

The range of h_w is 0 to 1. Bandt and Pompe [41] recommended $m = 3\sim7$ and $\tau = 1$. Considering the computational efficiency, $m = 3$ is selected in this paper. Similar to PE [42], WPE can also be used to distinguish between signal-dominant BLIMFs and noise-dominant BLIMFs.

2.4. Wavelet Threshold Denoising Method [4]. The essence of WTD is to filter the signal in the wavelet domain. Firstly, the signal is transformed into the wavelet domain. Then, the noisy wavelet coefficients are threshold processed. Finally, the denoised signal is reconstructed by wavelet coefficients. The primary steps of WTD are as follows:

(1) Decomposing the original signal by wavelet transform (WT) with proper wavelet basis function and decomposition level, and a group of wavelet decomposition coefficients are obtained.

(2) Selecting the appropriate threshold value to process the wavelet decomposition coefficient.

(3) The wavelet coefficients are reconstructed to get the denoised signal.

The selection of the threshold has a crucial impact on WTD. There are two common threshold denoising methods: wavelet hard threshold denoising (WHSD) and wavelet soft threshold denoising (WSTD) [4]. After WHSD, the signal is discontinuous, and the reconstructed signal will produce oscillation, while WSTD has better continuity. Therefore, WSTD is adopted in this paper.

2.5. Singular Spectrum Analysis. SSA proposed by Broomhead and King [34] is an effective method for analyzing and predicting nonlinear time series, which is suitable for nonlinear and nonstationary signal processing. For a given one-dimensional time series $\{q_t\}_{t=1}^{N}$, after selecting the appropriate window length L, $L \in [2, N]$, the trajectory matrix can be obtained by using the data embedding method, which can be expressed as

$$\mathbf{Q} = \begin{bmatrix} q_1 & q_2 & \cdots & q_M \\ q_2 & q_3 & \cdots & q_{M+1} \\ \vdots & \vdots & \vdots & \vdots \\ q_L & q_{L+1} & \cdots & q_N \end{bmatrix}, \tag{16}$$

where $M = N - L + 1$.

Then, the singular value decomposition (SVD) of $\mathbf{QQ}^{\mathrm{T}}$ can be written as

$$\mathbf{Q} = \sum_{i=1}^{d}\mathbf{Q}_i = \sum_{i=1}^{d}\sqrt{\lambda_i}\mathbf{U}_i\mathbf{V}_i^{\mathrm{T}}, \tag{17}$$

where d is the number of nonzero singular values of $\mathbf{QQ}^{\mathrm{T}}$, $\mathbf{Q}_i$ is the elementary matrices, $\lambda_1, \lambda_2, \ldots, \lambda_d$ is the singular values of $\mathbf{QQ}^{\mathrm{T}}$ arranged in descending order, and U_i and V_i are the ith left and right eigen vectors of $\mathbf{QQ}^{\mathrm{T}}$, respectively.

Based on the grouping principle, the set of indices $\{1, 2, \ldots, d\}$ are partitioned into G irrelevant subsets $I_1, I_2, \ldots, I_G$. Let $I_i = \{i_1, i_2, \ldots, i_c\}$ be the ith subset, the subset matrix and the trajectory matrix can be expressed as

$$\begin{aligned} \mathbf{Q}_{I_i} &= \mathbf{Q}_{i_1} + \mathbf{Q}_{i_2} + \cdots + \mathbf{Q}_{i_c}, \\ \mathbf{Q} &= \mathbf{Q}_{I_1} + \mathbf{Q}_{I_2} + \cdots + \mathbf{Q}_{I_G}. \end{aligned} \tag{18}$$

By applying the diagonal averaging method to $\mathbf{Q}_{I_i} = (q_{ij})_{(L\times M)}$, the bth element of signal reconstruction components RC_{I_i} is given by

$$\mathrm{RC}_b = \begin{cases} \dfrac{1}{b}\displaystyle\sum_{m=1}^{b} q^*_{m,b-m+1}, & 1 \le b < L^*, \\ \dfrac{1}{L^*}\displaystyle\sum_{m=1}^{L^*} q^*_{m,b-m+1}, & L^* \le b < K^*, \\ \dfrac{1}{N-b+1}\displaystyle\sum_{m=b-K^*+1}^{N-K^*+1} q^*_{m,b-m+1}, & K^* \le b < N, \end{cases} \tag{19}$$

where $L^* = \min(L, M)$, $K^* = \max(L, M)$, and

$$q_{ij}^{*} = \begin{cases} q_{ij}, & L < M, \\ q_{ji}, & M \le L. \end{cases} \tag{20}$$

It is worth noting that the window length L should be carefully selected because it directly affects the decomposition. However, there is no universal rule for the selection of the window length L. Through a large number of simulation experiments, we find that when the window length L is larger than $N/10$, the denoising performance of the proposed method is good enough. Considering the computational efficiency, $L = N/10$ is adopted in this paper.

Furthermore, the grouping principle is very important in SSA. In this paper, the noisy signal is divided into signal-dominant and noise-dominant components by singular entropy increment [36], and its computational equation is given by

$$I_i = -\left(\frac{\lambda_i}{\sum_{j=1}^{d}\lambda_j}\right)\ln\left(\frac{\lambda_i}{\sum_{j=1}^{d}\lambda_j}\right), \quad i = 1, 2, \ldots, d. \tag{21}$$

3. VMD-WTD-SSA Denoising Procedure

The process of the new efficient denoising method proposed in this paper is shown in Figure 1. It consists of four main steps explained as follows:

(1) The noise level of the noisy signal is obtained by using DFA. Then, MIE is used to determine the mode number for adaptive VMD denoising. At the same time, the noisy signal is decomposed into a series of BLIMFs by VMD, whose frequency increases gradually. The noise mainly concentrates in high frequency, and the useful signal is mainly concentrated in the first few BLIMFs.

(2) The WPE of each BLIMF is calculated. If the WPE is less than 0.4, the corresponding BLIMF will be regarded as the signal-dominant component. Otherwise, the corresponding BLIMF will be regarded as the noise-dominant component.

(3) The denoised signal by VMD is obtained by reconstructing the signal-dominant BLIMFs. Then, the denoised signal by VMD-WTD is obtained by reconstructing the signal-dominant BLIMFs and the noise-dominant BLIMFs, which have been denoised by WTD.

(4) The SSA is carried out for the denoised signal by VMD-WTD to obtain the denoised signal by VMD-WTD-SSA.

4. Simulation Signal Denoising

4.1. Construction of Simulation Signal. In order to verify the performance of the method proposed in this paper, the simulation data are tested. The equation of the noisy signal is as follows:

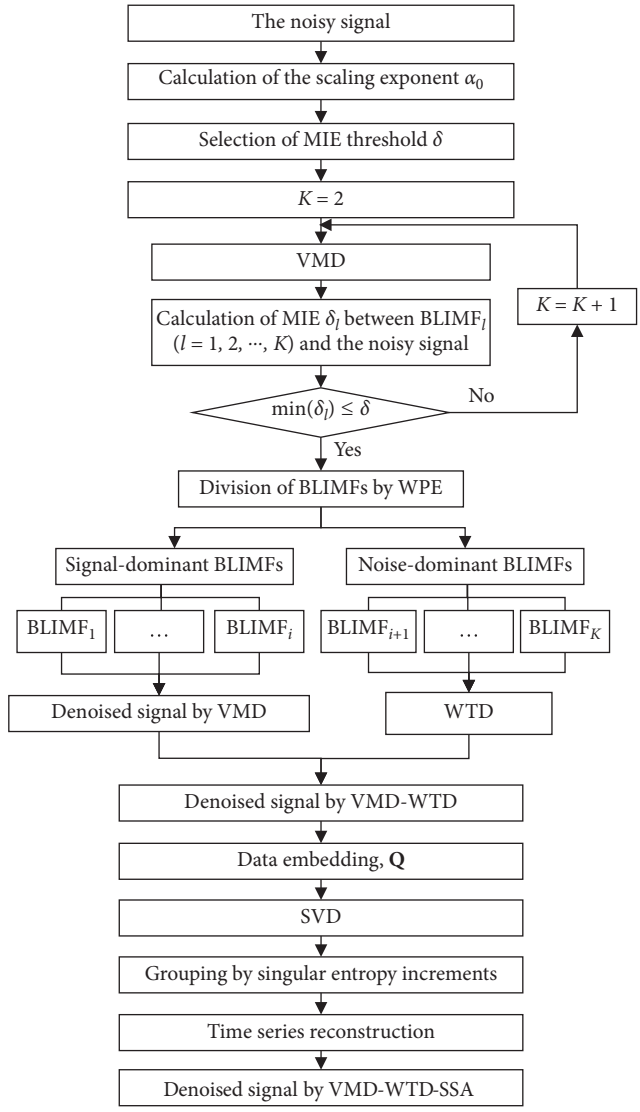

Figure 1: Flow chart of the proposed denoising method.

$$\begin{cases} x(t) = \cos(2\pi f_1 t) + 0.3\cos(2\pi f_2 t) + 0.02\cos(2\pi f_3 t), \\ x'(t) = x(t) + n', \end{cases} \tag{22}$$

where $f_1 = 5$, $f_2 = 20$, and $f_3 = 150$ represent the three frequencies of noise-free signal $x(t)$, and n' is the Gaussian white noise with a signal-to-noise ratio of 10 dB. The sampling frequency is 1000 Hz. The noisy and noise-free signals are shown in Figure 2.

4.2. Denoising of Simulation Signal. The scaling exponent α_0 of the noisy signal is 1.22, and the normalized MIE threshold δ is 0.015 by formula (9). Then, the normalized MIE between each BLIMF and the noisy signal (as defined in equation (8)) is obtained, as shown in Table 1.

It can be seen that the optimal mode number K is 10, and VMD is carried out for the simulation signal, and the BLIMFs are shown in Figure 3.

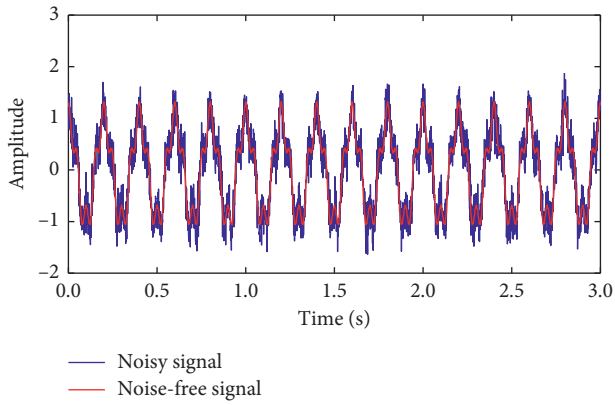

Figure 2: Simulation signal.

Table 1: Normalized MIE between each component and the noisy signal.

VMD	MIE
$BLIMF_1$	1
$BLIMF_2$	0.1336
$BLIMF_3$	0.0119
$BLIMF_4$	0.0223
$BLIMF_5$	0.0224
$BLIMF_6$	0.0333
$BLIMF_7$	0.0187
$BLIMF_8$	0.0178
$BLIMF_9$	0.0180
$BLIMF_{10}$	0.0257

The WPE of each BLIMF is shown in Table 2. Obviously, $BLIMF_1$ and $BLIMF_2$ are signal-dominant BLIMFs, and the rest of the BLIMFs are noise-dominant BLIMFs. Then, the $BLIMF_1$ and $BLIMF_2$ are reconstructed to get the denoised signal by VMD, as shown in Figure 4. It can be seen that after VMD denoising, the signal appears with partial distortion and oscillation.

WTD is conducted for the noise-dominant BLIMFs. In this paper, the db3 wavelet is selected and the number of decomposition levels is 3. Signal-dominant BLIMFs and noise-dominant BLIMFs after WTD are combined for signal reconstruction. VMD-WTD denoising performance is as shown in Figure 5. Obviously, the partial distortion and oscillation still exist, which demonstrates that the signal denoising performance after VMD-WTD denoising is still not ideal.

SSA is implemented for the denoised signal by VMD-WTD, and Figure 6 shows singular entropy increments ΔE of the signal. It is found that the information quantity of the signal reaches the saturated state at order 4, so the first 4 elementary matrices are used for reconstruction. After diagonal averaging, the denoised signal by VMD-WTD-SSA is obtained, as shown in Figure 7. It can be seen that the signal waveform is well recovered after denoising. Through the comparison, it can be seen that VMD-WTD-SSA denoising performance is superior to VMD and VMD-WTD denoising performances obviously.

4.3. Comparison with Other Methods. In this paper, the signal-to-noise ratio (SNR), root mean square error (RMSE), and maximum absolute error (MAE) are used as the evaluation indexes of denoising performance. SNR reflects the performance of the denoising method, and the larger the value, the better the denoising performance; RMSE reflects the similarity between the denoised signal and the noise-free signal, and the smaller the value, the better the denoising performance; MAE reflects the real error between the denoised signal and the noise-free signal, and the smaller the value, the better the denoising performance. The three evaluation indexes are defined as follows:

$$\begin{aligned} \mathrm{SNR} &= 10\log\left(\frac{\sum_{i=1}^{n} y^2(t)}{\sum_{i=1}^{n}\left[y(t) - y(t)\right]^2}\right), \\ \mathrm{RMSE} &= \sqrt{\frac{1}{n}\sum_{i=1}^{n}\left[y(t) - y'(t)\right]^2}, \\ \mathrm{MAE} &= \frac{1}{n}\sum_{i=1}^{n}\left|y(t) - y'(t)\right|, \end{aligned} \tag{23}$$

where $y(t)$ is the original signal, $y'(t)$ is the denoised signal, and n is the length of the original signal.

Six typical denoising methods are selected to compare with VMD-WTD-SSA. They are wavelet soft threshold denoising (WSTD) [4], EMD hard threshold denoising (EMD-HT) [11], EMD partial reconstruction (EMD-PR) [12], DFA-VMD [26], VMD-WTD [27], and VMD-AE [30]. Denoising results of different methods for the noisy signals with SNR_{in} values varying from −10 dB to 20 dB are shown in Figure 8. It can be seen that compared with the other methods, VMD-WTD-SSA has higher SNR_{out} and lower RMSE and MAE. Therefore, the results show that the VMD-WTD-SSA proposed in this paper has the best denoising performances with different SNR_{in} values. The presented method is better than the other methods on the whole, and its performance on noisy signals with low SNR is more prominent. Besides, as the SNR_{in} values continuously increases, the differences among these methods are narrowed.

5. Application to Load Signals

5.1. Acquisition of Load Signals. The signal acquisition system for the load test of a corn combine harvester is mainly composed of sensors (strain gauges and strain rosettes), an HBM data collecting instrument, and a computer, as shown in Figure 9.

According to existing experience, positions with large stress are determined as the measuring locations, of which the strain signals are measured by sensors. The layout of measuring locations of the frame is shown in Figure 10. There are six measuring locations in total.

The sampling frequency of strain signals is 500 Hz, which can fully meet the engineering test. In order to study the fatigue durability of the frame of a corn combine harvester, it is necessary to obtain the load data of the frame under multiple working conditions, such as cement road, field

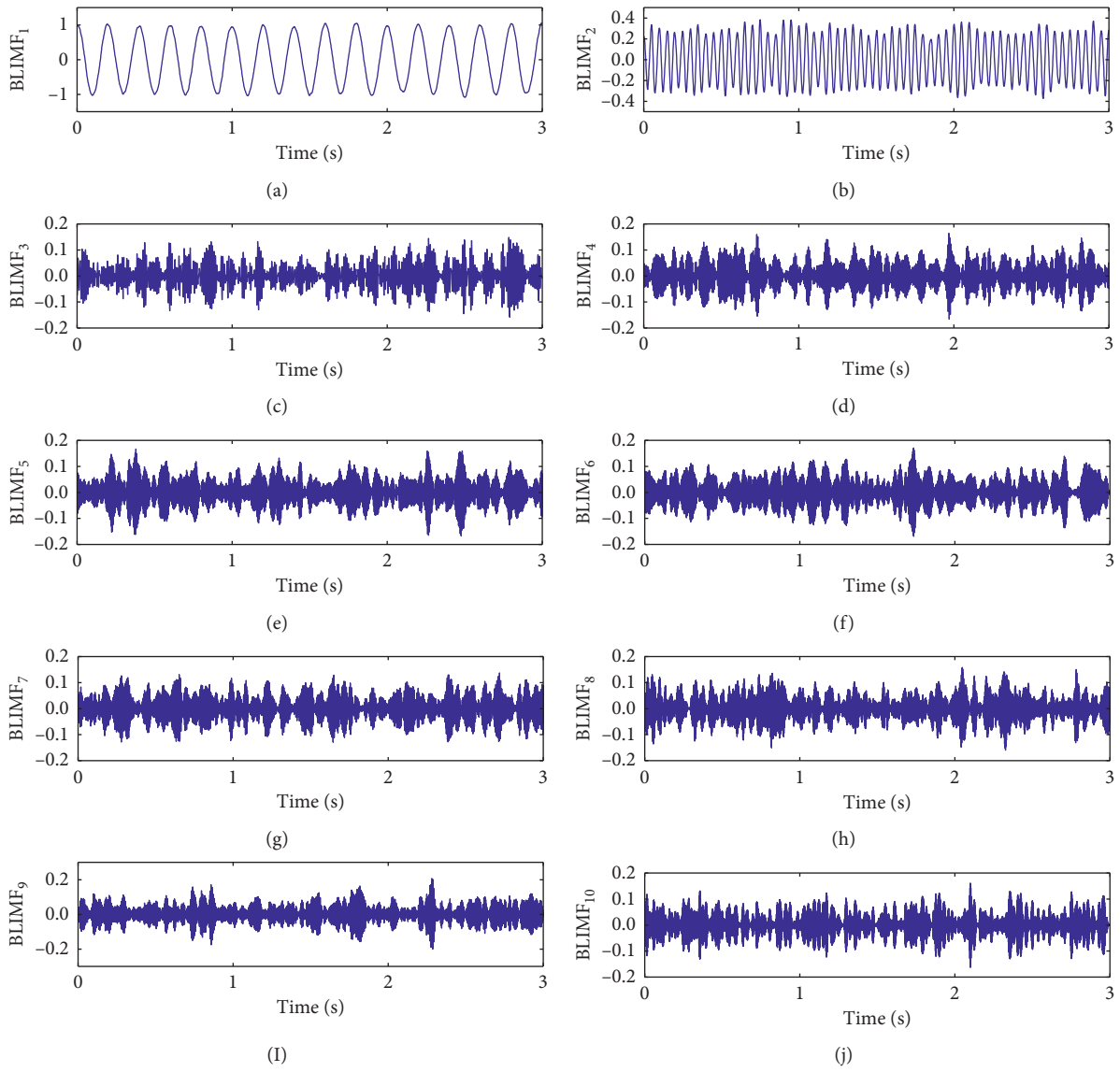

Figure 3: Decomposition results of the noisy signal. (a) BLIMF1. (b) BLIMF2. (c) BLIMF3. (d) BLIMF4. (e) BLIMF5. (f) BLIMF6. (g) BLIMF7. (h) BLIMF8. (I) BLIMF9. (j) BLIMF10.

Table 2: WPE of BLIMFs.

VMD	WPE
$BLIMF_1$	0.3870
$BLIMF_2$	0.3884
$BLIMF_3$	0.4629
$BLIMF_4$	0.5748
$BLIMF_5$	0.7058
$BLIMF_6$	0.8608
$BLIMF_7$	0.9678
$BLIMF_8$	0.9934
$BLIMF_9$	0.8672
$BLIMF_{10}$	0.7787

road, and gravel road. The load data under the field working condition is the most representative, which is used in the following analysis. Besides, working sections of a corn combine harvester under the field condition include straight-line harvesting sections and turning sections.

5.2. Denoising of Measured Signals. The method, proposed in this paper, is used to process the measured signal segment at location 5 in the straight-line harvesting section, which is shown in Figure 11. The scaling exponent α_0 of the noisy signal is 1.49, and the normalized MIE threshold is 0.015 by equation (9). It is determined that the mode number K is 6 by MIE, and VMD is carried out for the signal, as shown in Figure 12.

Then, the first four BLIMFs are determined as the signal-dominant BLIMFs by WPE. Therefore, the last two BLIMFs after WTD processing are combined with the first four BLIMFs to get the denoised signal by VMD-WTD. After that, SSA is implemented for the denoised signal by VMD-WTD, whose singular entropy increments ΔE are shown in

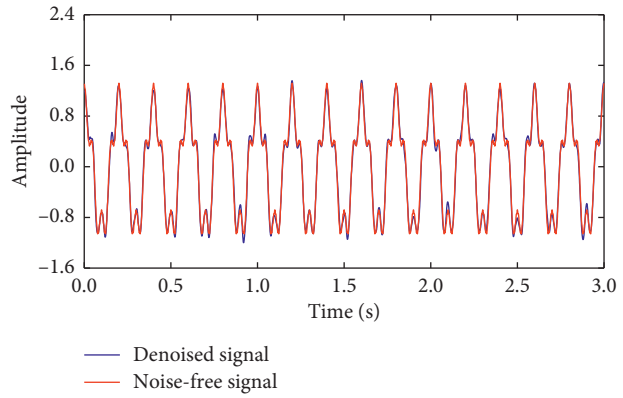

Figure 4: Comparison of the noise-free signal and the denoised signal by VMD.

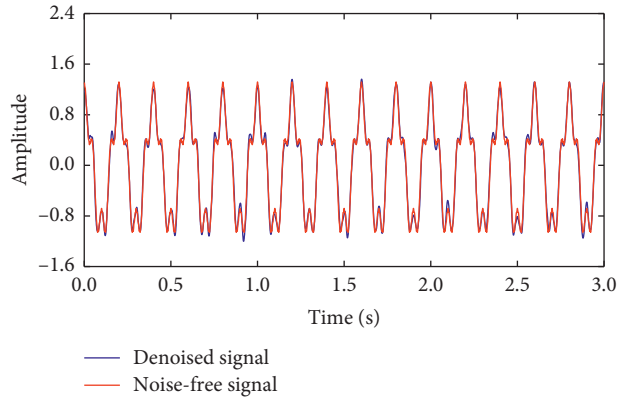

Figure 5: Comparison of the noise-free signal and the denoised signal by VMD-WTD.

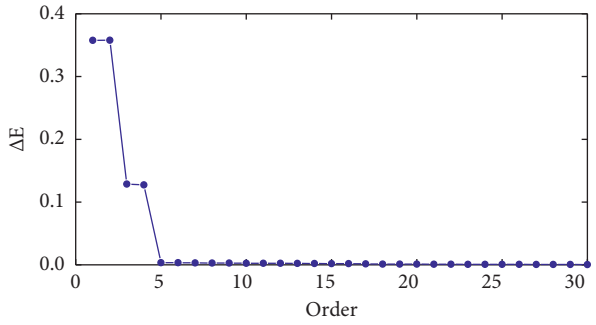

Figure 6: Singular entropy increments of the denoised signal by VMD-WTD.

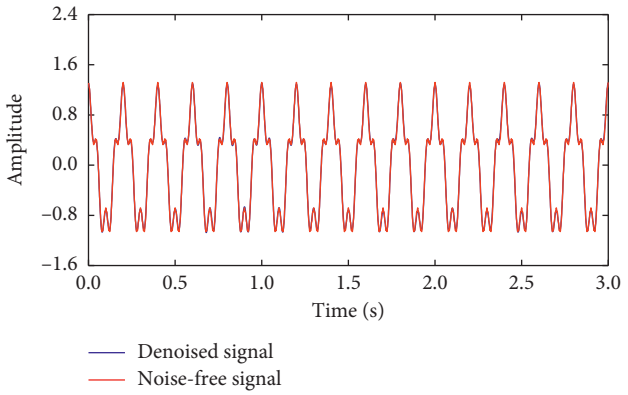

Figure 7: Comparison of the noise-free signal and the denoised signal by VMD-WTD-SSA.

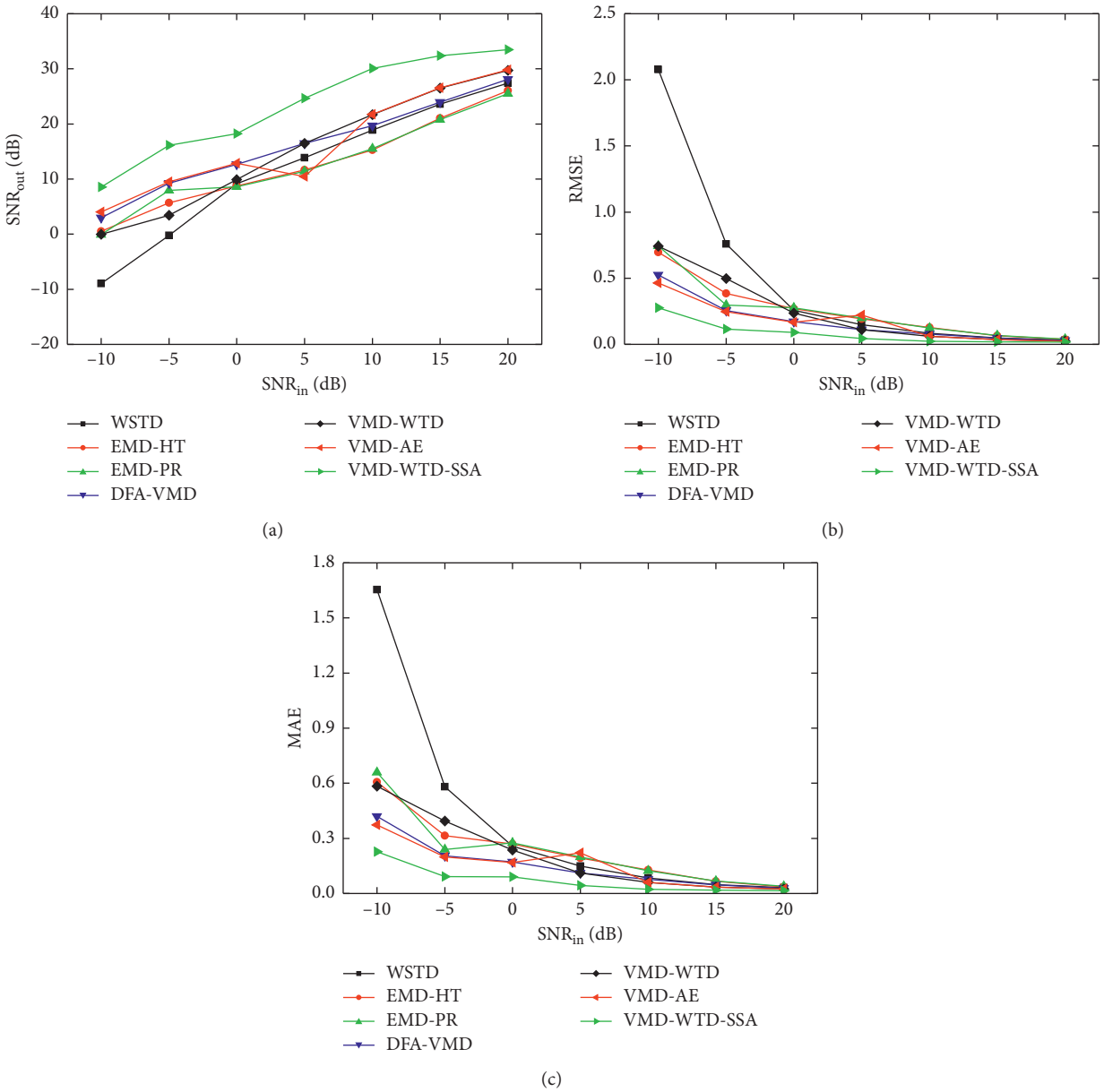

Figure 8: Denoising results for simulation signals with different SNR$_{in}$: (a) SNR$_{out}$, (b) RMSE, and (c) MAE.

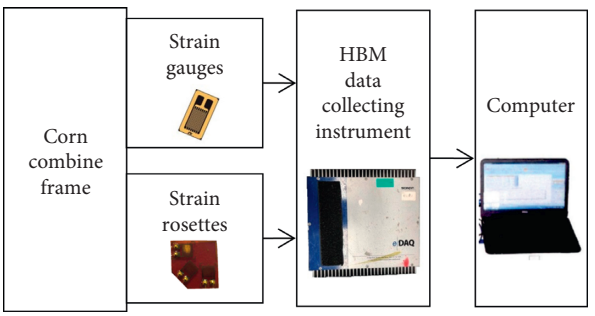

Figure 9: Signal acquisition system.

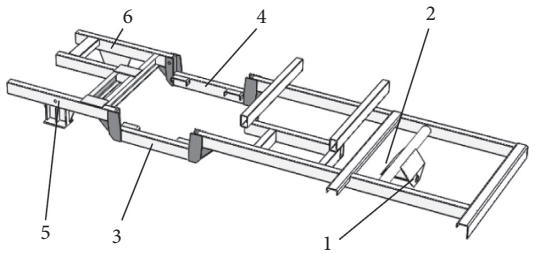

Figure 10: Layout of measurement locations of the frame.

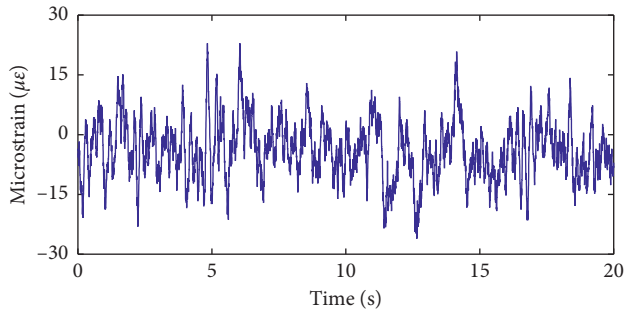

Figure 11: Measured signal in the straight-line harvesting section.

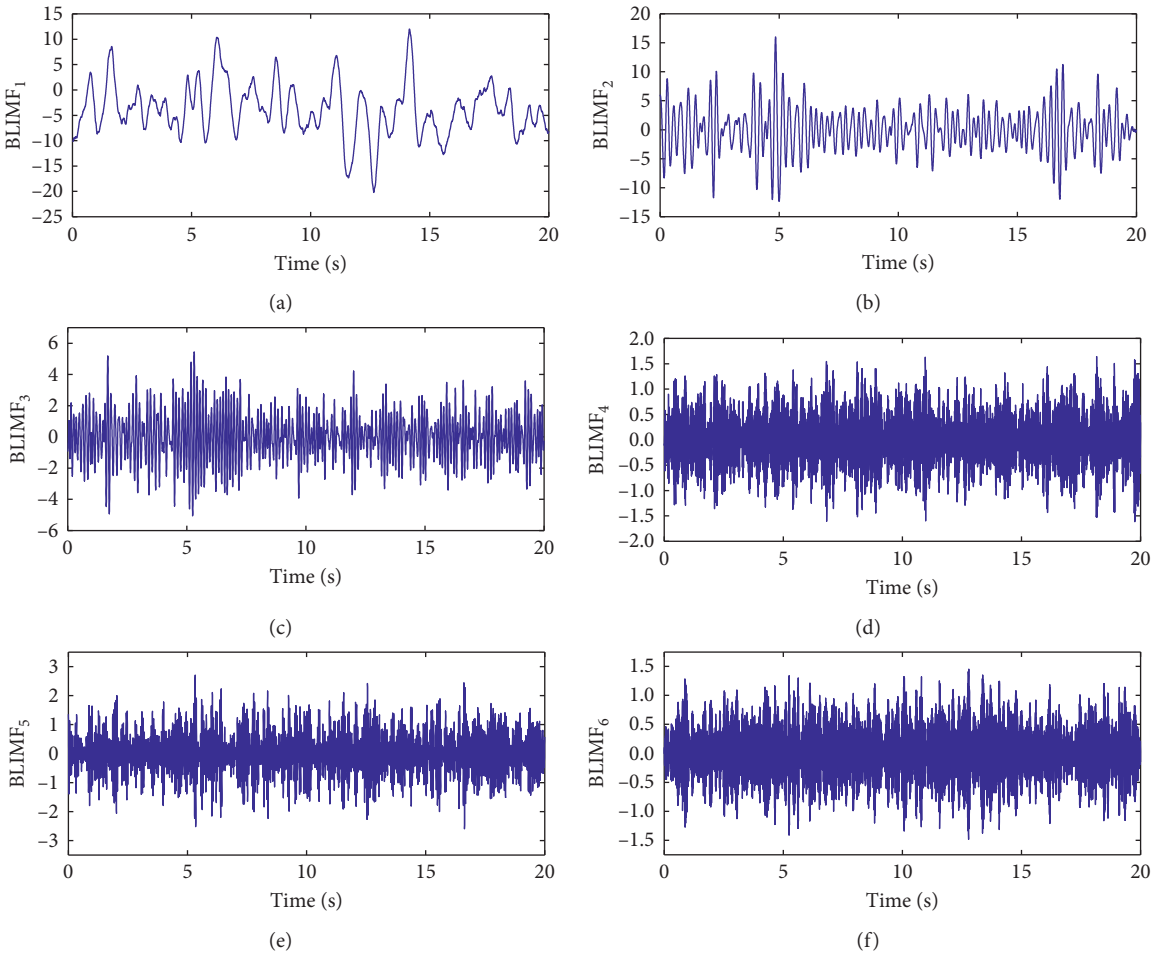

Figure 12: Decomposition results of the measured signal in the straight-line harvesting section. (a) BLIMF1. (b) BLIMF2. (c) BLIMF3. (d) BLIMF4. (e) BLIMF5. (f) BLIMF6.

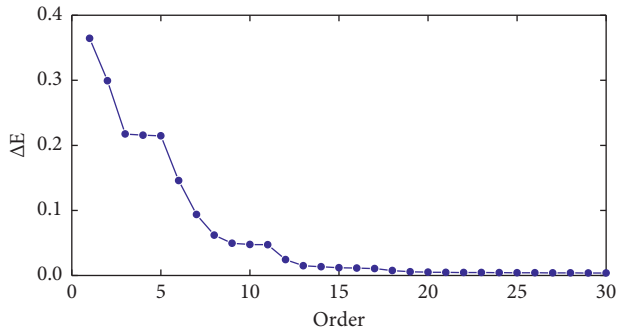

Figure 13: Singular entropy increments of the measured signal in the working section of linear harvesting.

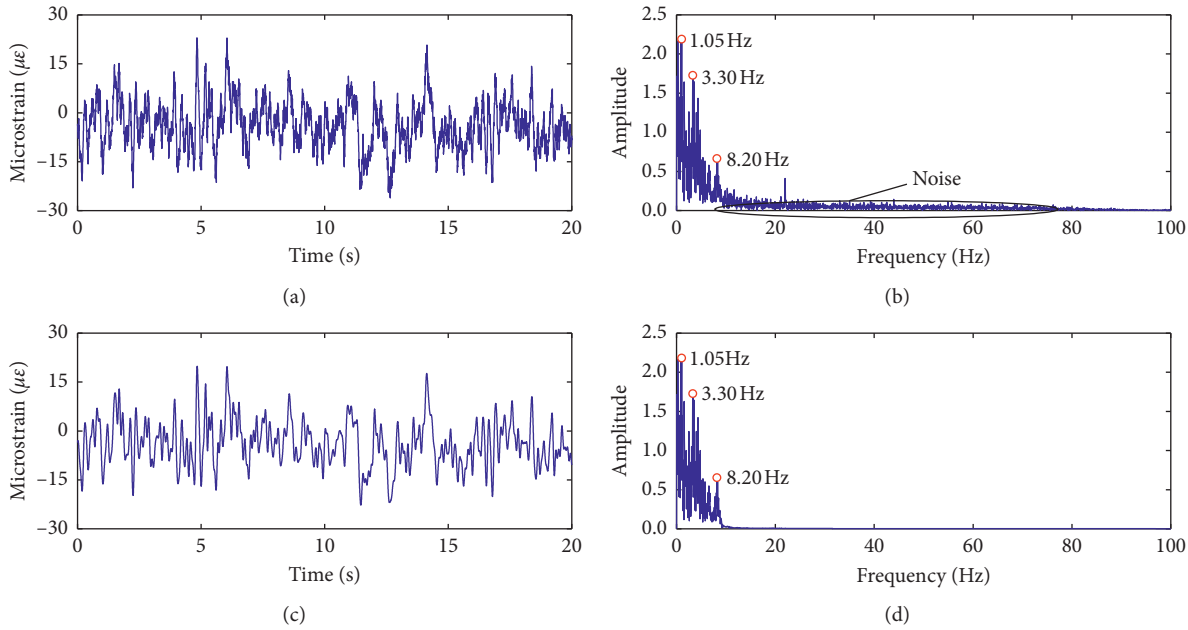

Figure 14: Comparison before and after denoising of the measured signal in the working section of linear harvesting: (a) measured signal, (b) spectra diagram of the measured signal, (c) denoised signal, and (d) spectra diagram of the denoised signal.

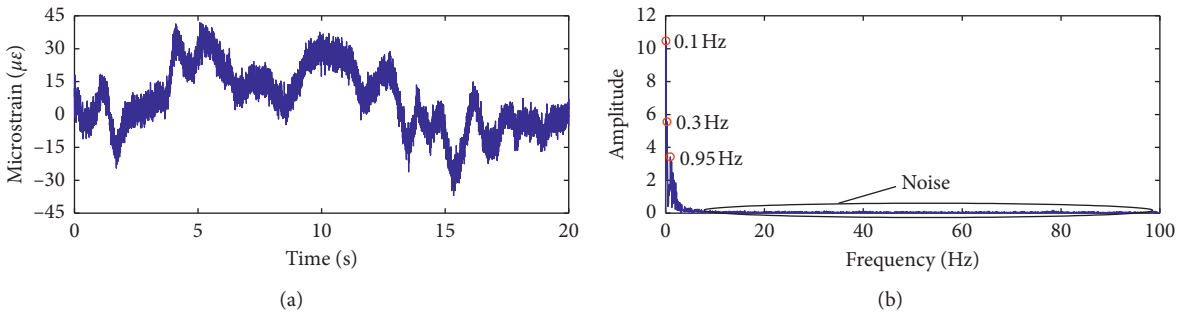

Figure 15: Continued.

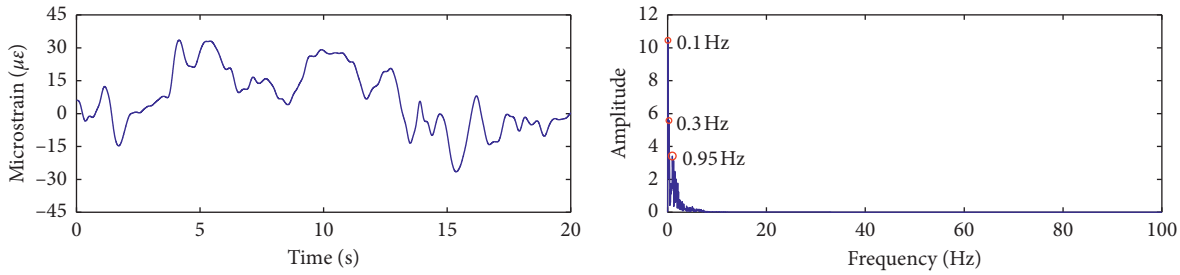

Figure 15: Comparison before and after denoising of the measured signal in the working section of turning: (a) measured signal, (b) spectra diagram of the measured signal, (c) denoised signal, and (d) spectra diagram of the denoised signal.

Figure 13. It is found that the information quantity of the signal reaches the saturated state at order 11, so the first 11 elementary matrices are used for reconstruction. After diagonal averaging, the denoised signal by VMD-WTD-SSA is obtained, which is shown in Figure 14(a).

The measured signals in different sections and their spectra before and after denoising are compared, as shown in Figures 14 and 15. It can be seen that the denoised signals by VMD-WTD-SSA not only retain the low-frequency effective components of the original signal but also eliminate the interference of high-frequency noise, which fully shows the superiority of the proposed method. Therefore, the denoising method proposed in this paper has a significant denoising performance on time domain load signals, which lays the foundation for further analysis and processing.

6. Conclusion

In order to improve the denoising performance of time domain load signals, an efficient denoising method based on VMD, WTD, and SSA is proposed in this paper. Firstly, a simple criterion including MIE and the scaling exponent α_0, which can be obtained by using DFA, is designed to select the proper mode number K for VMD. In addition, the BLIMFs are divided into the noise-dominate and signal-dominate parts by using WPE, which can help identify the useful information from the noisy signal. Furthermore, the presented method takes full advantages of VMD, WTD, and SSA, which can suppress noise and retain useful components of the original signal. The denoising performance of the proposed method is quantitatively evaluated by using the simulation signals, which are composed of different frequency components and Gaussian white noise. Experimental results of the presented simulation signals with SNR_{in} values varying from −10 dB to 20 dB demonstrate that the proposed method outperforms WSTD, EMD-HT, EMD-PR, DFA-VMD, VMD-WTD, and VMD-AE. Moreover, applied to measured load signals, the presented method can not only effectively remove the noise component but also retain the effective component of the original signal, which proves its feasibility.

Although the effectiveness of the proposed method has been verified by the denoising results of synthetic and measured signals, its universality is worth investigating further through a large number of simulation signals, which are comprised of various original signals and noise. Besides, the feasibility of the proposed method is qualitatively evaluated by the spectra diagrams of denoised measured load signals. Nevertheless, the influence of the denoising process on the fatigue durability analysis of mechanical structures needs to be further studied. Further work will be carried out to study the universality of the presented approach and apply the denoised measured load signals to the fatigue durability analysis of mechanical structures.

Data Availability

The time domain load signals used to support the findings of this study are included within the supplementary information file.

Conflicts of Interest

The authors declare that there are no conflicts of interest regarding the publication of this paper.

Acknowledgments

This research was funded by the National Key Research and Development Plan of China (2017YFD0700301).

Supplementary Materials

Supplementary Materials: time domain load signals of the corn combine frame under the field condition, which includes the straight-line harvesting section and the turning section. The lengths of them are 20 s and 40 s, respectively. (*Supplementary Materials*)

References

[1] W. Li, S. Zhou, Z. Shi, X. Wang, and P. Hu, "Experimental and numerical analysis on fatigue durability of single-lap joints under vibration loads," *The Journal of Adhesion*, vol. 93, no. 3, pp. 187–203, 2017.

[2] N. Lu, G. Zhang, Y. Cheng, and D. Chen, "Signal denoising method based on adaptive redundant second-generation wavelet for rotating machinery fault diagnosis," *Mathematical Problems in Engineering*, vol. 2016, Article ID 2727684, 10 pages, 2016.

[3] Y. Li, Y. Li, X. Chen, and J. Yu, "Research on ship-radiated noise denoising using secondary variational mode decomposition and correlation coefficient," *Sensors*, vol. 18, no. 1, p. 48, 2018.

[4] D. L. Donoho and I. M. Johnstone, "Ideal spatial adaptation by wavelet shrinkage," *Biometrika*, vol. 81, no. 3, pp. 425–455, 1994.

[5] Z. Wang, J. Luo, Y. Liu, and S. Cai, "Wavelet denoising of vehicle platform vibration signal based on threshold neural network," *Shock and Vibration*, vol. 2017, Article ID 7962828, 12 pages, 2017.

[6] H.-Y. Lin, S.-Y. Liang, Y.-L. Ho, Y.-H. Lin, and H.-P. Ma, "Discrete-wavelet-transform-based noise removal and feature extraction for ECG signals," *IRBM*, vol. 35, no. 6, pp. 351–361, 2014.

[7] S. Madhur, G. Elka R, and F. Jack H, "A new wavelet denoising method for experimental time-domain signals: pulsed dipolar electron spin resonance," *Journal of Physical Chemistry A*, vol. 121, no. 12, pp. 2452–2465, 2017.

[8] H. Liu, W. Wang, C. Xiang, L. Han, and H. Nie, "A de-noising method using the improved wavelet threshold function based on noise variance estimation," *Mechanical Systems and Signal Processing*, vol. 99, pp. 30–46, 2018.

[9] N. E. Huang, Z. Shen, S. R. Long et al., "The empirical mode decomposition and the Hilbert spectrum for nonlinear and non-stationary time series analysis," *Proceedings of the Royal Society of London. Series A: Mathematical, Physical and Engineering Sciences*, vol. 454, no. 1971, pp. 903–995, 1998.

[10] A. O. Boudraa, J. C. Cexus, and Z. Saidi, "EMD-based signal noise reduction," *International Journal of Signal Processing*, vol. 1, no. 1, pp. 33–37, 2004.

[11] K. Khaldi, A. O. Boudraa, A. Bouchikhi, M. T. H. Alouane, and E. H. S. Diop, "Speech signal noise reduction by EMD," in *Proceedings of the 2008 3rd International Symposium on Communications, Control and Signal Processing*, pp. 1155–1158, IEEE, St Julians, Malta, March 2008.

[12] A.-O. Boudraa and J.-C. Cexus, "EMD-based signal filtering," *IEEE Transactions on Instrumentation and Measurement*, vol. 56, no. 6, pp. 2196–2202, 2007.

[13] Z. Xu, B. Huang, and F. Zhang, "Improvement of empirical mode decomposition under low sampling rate," *Signal Processing*, vol. 89, no. 11, pp. 2296–2303, 2009.

[14] J. Zheng, J. Cheng, and Y. Yang, "Generalized empirical mode decomposition and its applications to rolling element bearing fault diagnosis," *Mechanical Systems and Signal Processing*, vol. 40, no. 1, pp. 136–153, 2013.

[15] X. Hu, S. Peng, and W. Hwang, "EMD revisited: a new understanding of the envelope and resolving the mode-mixing problem in AM-FM signals," *IEEE Transactions on Signal Processing*, vol. 60, no. 3, pp. 1075–1086, 2012.

[16] Q. Liu, Z. Tan, Y. Zhang, and H. Wang, "Denoising of fetal heart sound based on empirical mode decomposition method," *Journal of Biomedical Engineering*, vol. 32, no. 4, pp. 740–745, 2015.

[17] Z. Wu and N. E. Huang, "Ensemble empirical mode decomposition: a noise-assisted data analysis method," *Advances in Adaptive Data Analysis*, vol. 1, no. 1, pp. 1–41, 2009.

[18] J.-R. Yeh, J.-S. Shieh, and N. E. Huang, "Complementary ensemble empirical mode decomposition: a novel noise enhanced data analysis method," *Advances in Adaptive Data Analysis*, vol. 2, no. 2, pp. 135–156, 2010.

[19] J. Zhang, J. He, J. Long, M. Yao, and W. Zhou, "A new denoising method for UHF PD signals using adaptive VMD and SSA-based shrinkage method," *Sensors*, vol. 19, no. 9, p. 1594, 2019.

[20] Y. Li, Y. Li, X. Chen, and J. Yu, "A novel feature extraction method for ship-radiated noise based on variational mode decomposition and multi-scale permutation entropy," *Entropy*, vol. 19, no. 7, p. 342, 2017.

[21] K. Dragomiretskiy and D. Zosso, "Variational mode decomposition," *IEEE Transactions on Signal Processing*, vol. 62, no. 3, pp. 531–544, 2014.

[22] Y. Li, X. Chen, J. Yu, and X. Yang, "A fusion frequency feature extraction method for underwater acoustic signal based on variational mode decomposition, duffing chaotic oscillator and a kind of permutation entropy," *Electronics*, vol. 8, no. 1, Article ID 61, 2019.

[23] Y. Li, Y. Li, X. Chen, and J. Yu, "Denoising and feature extraction algorithms using NPE combined with VMD and their applications in ship-radiated noise," *Symmetry*, vol. 9, no. 11, p. 256, 2017.

[24] F. Li, B. Zhang, S. Verma, and K. J. Marfurt, "Seismic signal denoising using thresholded variational mode decomposition," *Exploration Geophysics*, vol. 49, no. 4, pp. 450–461, 2018.

[25] T. Hua, K. Dai, X. Zhang et al., "Optimal VMD-based signal denoising for laser radar via Hausdorff distance and wavelet transform," *IEEE Access*, vol. 7, pp. 167997–168010, 2019.

[26] Y. Liu, G. Yang, M. Li, and H. Yin, "Variational mode decomposition denoising combined the detrended fluctuation analysis," *Signal Processing*, vol. 125, pp. 349–364, 2016.

[27] Z. Lei, W. Su, and Q. Hu, "Multimode decomposition and wavelet threshold denoising of mold level based on mutual information entropy," *Entropy*, vol. 21, no. 2, p. 202, 2019.

[28] Y. Li, X. Chen, J. Yu, X. Yang, and H. Yang, "The data-driven optimization method and its application in feature extraction of ship-radiated noise with sample entropy," *Energies*, vol. 12, no. 3, p. 359, 2019.

[29] X. Yu, L. Pan, and X. An, "Denoising algorithm of pressure fluctuation signals of hydraulic turbines based on VMD and permutation entropy," *Journal of Hydroelectric Engineering*, vol. 36, no. 8, pp. 78–85, 2017.

[30] X. An and J. Yang, "Denoising of hydropower unit vibration signal based on variational mode decomposition and approximate entropy," *Transactions of the Institute of Measurement and Control*, vol. 38, no. 3, pp. 282–292, 2016.

[31] W. Ma, S. Yin, C. Jiang, and Y. Zhang, "Variational mode decomposition denoising combined with the Hausdorff distance," *Review of Scientific Instruments*, vol. 88, no. 3, Article ID 035109, 2017.

[32] G. Ren, J. Jia, J. Mei, X. Jia, and J. Han, "Variational mode decomposition denoising combined with the Euclidean distance for diesel engine vibration signal," *Journal of Vibroengineering*, vol. 20, no. 5, pp. 2045–2059, 2018.

[33] B. Li, L. Zhang, Q. Zhang, and S. Yang, "An EEMD-Based denoising method for seismic signal of high arch dam combining wavelet with singular spectrum analysis," *Shock and Vibration*, vol. 2019, Article ID 4937595, 9 pages, 2019.

[34] D. S. Broomhead and G. P. King, "On the qualitative analysis of experimental dynamical systems," *Physica D: Nonlinear Phenomena*, vol. 20, no. 2-3, pp. 217–236, 1986.

[35] H. Hassani, "Singular spectrum analysis: methodology and comparison," *Journal of Data Science*, vol. 5, no. 2, pp. 239–257, 2007.

[36] W.-X. Yang and P. W. Tse, "Development of an advanced noise reduction method for vibration analysis based on singular value decomposition," *NDT & E International*, vol. 36, no. 6, pp. 419–432, 2003.

[37] C.-K. Peng, S. V. Buldyrev, S. Havlin, M. Simons, H. E. Stanley, and A. L. Goldberger, "Mosaic organization of DNA nucleotides," *Physical Review E*, vol. 49, no. 2, pp. 1685–1689, 1994.

[38] A. M. Fraser and H. L. Swinney, "Independent coordinates for strange attractors from mutual information," *Physical Review A*, vol. 33, no. 2, pp. 1134–1140, 1986.

[39] S. Leistedt, M. Dumont, J.-P. Lanquart, F. Jurysta, and P. Linkowski, "Characterization of the sleep EEG in acutely depressed men using detrended fluctuation analysis," *Clinical Neurophysiology*, vol. 118, no. 4, pp. 940–950, 2007.

[40] B. Fadlallah, B. Chen, A. Keil, and J. Principe, "Weighted-permutation entropy: a complexity measure for time series incorporating amplitude information," *Physical Review E*, vol. 87, no. 2, Article ID 022911, 2013.

[41] C. Bandt and B. Pompe, "Permutation entropy: a natural complexity measure for time series," *Physical Review Letters*, vol. 88, no. 17, Article ID 174102, 2002.

[42] S. Zhang, J. Tian, A. Banerjee, and J. Li, "An efficient porcine acoustic signal denoising technique based on EEMD-ICA-WTD," *Mathematical Problems in Engineering*, vol. 2019, Article ID 2858740, 12 pages, 2019.